Fire Safety Journal 59 (2013) 22–29

Contents lists available at SciVerse ScienceDirect

Fire Safety Journal

journal homepage: www.elsevier.com/locate/firesaf

Modeling of dust air flames

Scott R. Rockwell, Ali S. Rangwala *

Department of Fire Protection Engineering, Worcester Polytechnic Institute, Worcester, MA 01609, USA

ARTICLE INFO

Article history:
Received 29 January 2012
Received in revised form
19 September 2012
Accepted 18 March 2013
Available online 30 April 2013

Keywords:
Dust
Deflagration
Premixed-combustion
Particle–air flames

ABSTRACT

This study analyzes a premixed dust–air flame, under conditions where a homogeneous gas-phase reaction front can exist. Discussion on four possible flame types is provided. A solution is obtained for the burning velocity of a flammable dust–air flame in both fuel and oxygen limiting cases. A sensitivity analysis is used to analyze the features controlling the dust burning. It is shown that vaporization is significant for fuel limiting conditions; however, does not play a major role in oxygen limiting cases. The calculated burning velocity shows good agreement with available experimental data for coal–dust–air flames.

1. Introduction

In industries that make, transport, and/or use flammable dusts, accidental dust deflagrations represent a real hazard to both personnel and equipment. Over the last 20 years, advances in expanding chemical, metallurgical, and pharmaceutical industries have given birth to a steadily increasing number of new finely divided flammable materials [1]. In a recent review by Abbasi and Abbasi [2] dust deflagrations caused 125 casualties and 398 injuries between 1980 and 2003. These explosions caused by a wide range of dusts including grain, aluminum, coal, textile, rubber, resin, and others. The Occupational Safety & Health Administration (OSHA) [3] has further explored accidents involving dusts to show the problem is still at large. This study focuses on researching the problem from a fundamental perspective stressing a basic understanding about the premixed dust–air flame. This is achieved by subdividing the dust flame into four types based on the conditions in the ambient (unburned) and post-flame region. The classification allows systematic comparison with the gaseous fuel–air premixed flames studied extensively in literature.

2. Flame structure

The earliest work on dust–air premixed flames is provided by Nusselt [4] and the most up-to-date review on the topic is given by Eckhoff [1]. Smoot and Horton [5], Krazinski et al. [6], and Slezak et al. [7] have investigated the problem using numerical modeling. Unlike a premixed gas flame, a mixture of dust and oxidizer involves a multiphase flow which causes difficulty in both experiments and modeling [1,8,10–12]. For gases, the reactants are separated by molecular distances [13]. Premixed combustion is therefore guaranteed to small scales. By contrast, dust explosions and dust flames involve the combustion of a dust–air suspension. A dust cloud which is uniform when viewed at a macro-scale (e.g. cloud radius), may not be premixed at a small scale (e.g. interparticle distance). This caused researchers to make a distinction between two types of dust flames [1]: the Nusselt flame and the volatile flame. In the Nusselt flame, strictly heterogeneous combustion occurs at the surface of the particles, sustained by diffusing oxygen towards the particles' surface. Therefore, a Nusselt flame, which on a macroscopic scale may seem like premixed combustion, consists of an ensemble of local diffusion flames. Such flames are not considered in this study. With a volatile flame, particles produce vapor before combustion. When mixed with air, these gases and vapors burn as a premixed gas. Depending on the nature of the solid, three distinctive mechanisms have been proposed for the combustions of particles in volatile flames [14]:

1. Devolatilization and burning of volatiles followed by combustion of a solid residue.
2. Melting followed by evaporation and subsequently vapor phase burning.
3. Evaporation through a solid oxide shell followed by combustion of the vapor outside the shell.

Three steps of volatilization, mixing of the volatiles with air, and combustion of the mixture are necessary for flame

* Corresponding author. Tel.: +1 5088316409.
E-mail address: rangwala@wpi.edu (A.S. Rangwala).

0379-7112/$ - see front matter © 2013 Elsevier Ltd. All rights reserved.
http://dx.doi.org/10.1016/j.firesaf.2013.03.006

Nomenclature

A	parameter characterizing rate of vaporization of fuel particles [g/(m^2/K/s]
a	defined in Table 1
B	Arrhenius frequency factor [1/s]
c_p	specific heat [J/(kg/K)]
C_F	molar concentration of fuel [mol/m^3]
D	species mass diffusivity [m^2/s]
E	activation energy of the gas-phase reaction [J/mol]
k	rate constant of the gas-phase reaction [1/s]
W	molecular weight [g/mol]
n	temperature exponent characterizing rate of vaporization of fuel particles [–]
n_u	particle number density [1/m^3]
K_{st}	deflagration index [bar m/s]
P	pressure [bar]
Q	heat of reaction [J/kg]
Q_v	heat of vaporization [J/kg]
q	heat of vaporization/ heat of reaction [–]
R	gas constant [J/mol/K]
r	average particle radius [m]
S_i	sensitivity parameter [–]
S_L	laminar burning velocity [m/s]
T	temperature [K]
u	velocity [m/s]
x_0	defined in Eq. (9)
x_1	defined in Eq. (9)
Y	mass fraction [–]
y_o	defined in Eq. (9)
y_1	defined in Eq. (9)
Ze	Zeldovich number
α	defined in Table 1
ν	stoichiometric coefficient [–]
λ	thermal conductivity [W/m/K)]
ρ	density [kg/m^3]
ϕ_u	equivalence ratio based on the initial condensed phase fuel [–]
ϕ_g	equivalence ratio based on the volatized gas evolved at the end of the preheat zone [–]
γ	defined in Table 1
$\dot{w}'''_F$	gas-phase reaction rate [g/(m^3/s)]
$\dot{w}'''_v$	vaporization rate [g/(m^3/s)]

Subscripts

air	property of air
b	burned mixture
F	gaseous fuel
FC	fuel fraction in reaction zone
f	at the reaction zone/flame location
g	gas
max	maximum
mix	combined solid and gas-phase property
N	normalized variable
O	oxygen
s	solid fuel
st	stoichiometric
u	unburned mixture

propagation in a dust cloud. The first step, the release of volatiles from the fuel due to thermal degradation or surface reactions or a combination of both, is the most complicated due to the heterogeneous behavior. The three processes are illustrated in Fig. 1, where four potential scenarios (A, B, C_I and C_{II}) based on two equivalence ratios, ϕ_u and ϕ_g are presented; variable ϕ_u represents the equivalence ratio based on the total condensed phase fuel in the ambient zone, whereas ϕ_g represents the equivalence ratio based on the volatized gas vapor evolved at the end of the preheat zone.

In Fig. 1, label "A" denotes the condition where $\phi_u < 1$ and $\phi_g < 1$. Label "B" denotes the condition where ϕ_u can take any value but with the condition of $\phi_g < 1$. It is assumed here that the number of particles is large enough such that the flame standoff distance surrounding each particle is significantly larger than the characteristic separation distance between the particles. For liquid droplets (spray flames) this is observed for overall equivalence ratios (ϕ_u) greater than 0.7 [15]. Label "C" denotes the condition where both ϕ_u and ϕ_g are greater than 1. Two cases can arise, in this case: "C_I", where the particles completely vaporize in the preheat zone (burned mixture in convective zone comprises of fuel rich vapor), and "C_{II}" where the particles do not completely vaporize and act as heat sinks in the convective zone. The gray shading is shown to indicate the mass fraction of fuel vapor present with a darker color representing higher mass fraction.

The inset labeled "D" shows a close-up of the ambient zone where the random distribution of both particle separation and size in a dust–air flame is highlighted. In most models, including those

Table 1
Dust–air flame models.

No.	Model equations	ϕ_g range
1 Seshadri et al. [18]	$S_L^2 = \frac{2\nu_F\lambda_u B(1/Ze)^2}{\rho_u c_{p,mix}}\exp\left(-\frac{E}{RT_f}\right)$ $Y_{FC}Q = c_{p,mix}(T_f - T_u)$ $3a\alpha^{2/3} - 3a^2\alpha^{1/3} + a^3 - 1 = 0$	$\phi_g \leq 1$
2 This work	$S_L^2 = \frac{2\lambda_u B(1/Ze)^2}{\rho_u c_{p,mix}}\exp\left(-\frac{E}{RT_b}\right)$ $Y_{FC}Q = c_{p,mix}(T_f - T_u)$ $3a\alpha^{2/3} - 3a^2\alpha^{1/3} + a^3 - 1 = 0$	$\phi_g \geq 1$

$a = \frac{\gamma}{3n}$, $Ze = \frac{E(T_f - T_u)}{RT_f^2}$, $\alpha = \frac{Y_{Fu}}{Y_{FC}}$, $c_{p,mix} = \frac{\frac{\nu_F W_F Q}{\nu_O W_O} Y_{O,u}}{(T_b - T_u)}$, $\gamma = \frac{4.836 A n_u^{1/3}\lambda_u (T_f - T_u)^n}{S_L^2 \rho_u^{4/3} c_{p,mix} Y_{FC}^{1/3} \rho_s^{2/3}}$

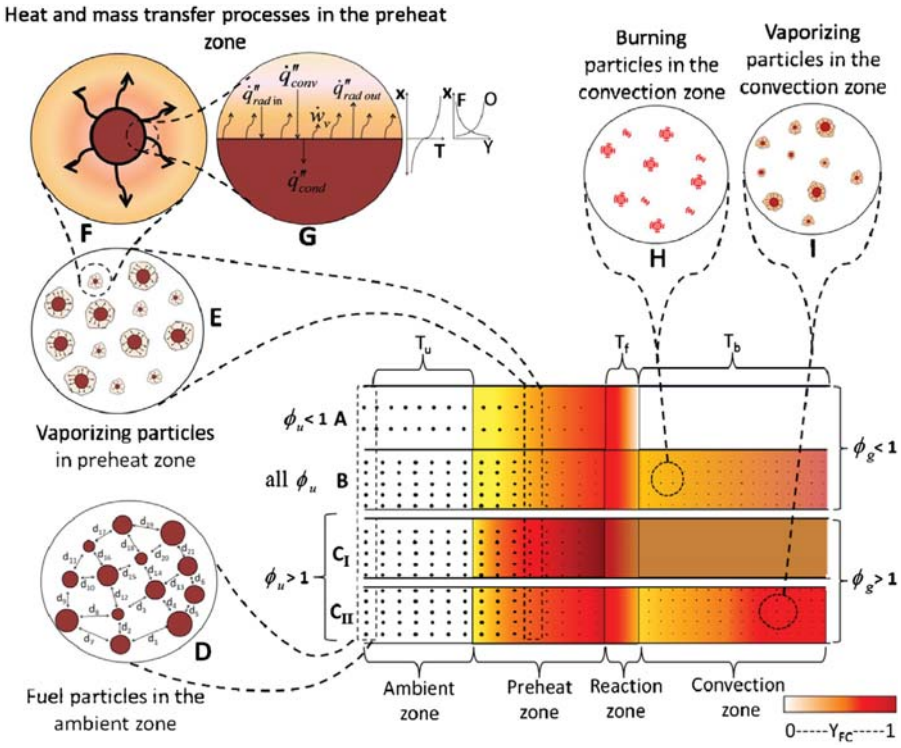

Fig. 1. Schematic illustration of the structure of a premixed dust–air flame.

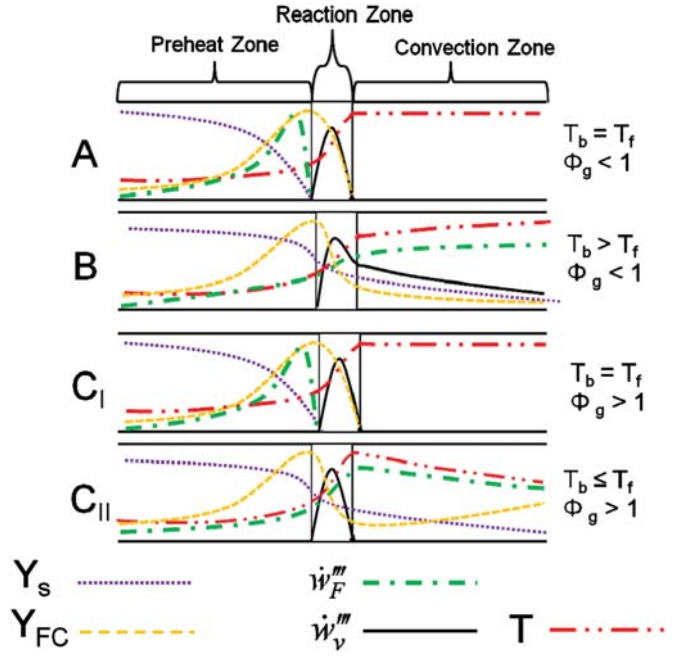

Fig. 2. Schematic of flame structure in a dust–air flame.

presented in this work, these quantities are approximated as average values, and it is assumed that there is an even distribution of particles of an average size and a single fuel type. The implications of this simplification have not been thoroughly investigated in the combustion literature, though there has been some research into deriving models for dual particle sizes [16] and dual particle fuels [17].

The inset labeled "E" shows a close-up of the preheat zone. During this, the differences in particle size play a significant role as smaller particles heat up faster and vaporize almost completely, while larger particles continue to be in the condensed phase as they move into the reaction and convection zones. The inset labeled "F" shows a close-up view of a single vaporizing particle with the inset labeled "G" showing the surface of a particle in the preheat zone where the fuel changes phase from solid to gas and premixes with the oxidizer to establish a flame front. At this stage, it is possible that burning is localized on the surface alone. Note that the change in phase slows down burning velocity significantly compared with a gas flame. Further, as shown in "G", the heat flux related to in-depth conduction ($\dot{q}''_{cond}$) and radiation ($\dot{q}''_{rad,in}$, $\dot{q}''_{rad,out}$) also play a significant role. The inset "G" also shows the vaporization rate ($\dot{w}'''_v$), which is determined by an energy balance of the net heat transfer divided by heat of gasification. These additional parameters influence the burning of particle air flames as discussed further in Fig. 2, which shows a sketch of the flame structure for the four types of equivalence ratio combinations considered.

The profiles of mass fraction of condense-phase fuel (Y_s), mass fraction of vaporized fuel (Y_{FC}), the vaporization rate ($\dot{w}'''_v$), the reaction rate ($\dot{\omega}'''_R$), and the temperature (T), across ambient, preheat, reaction and convection zones, are shown in Fig. 2. Case I represents the conditions where $\phi_g \leq 1$ and all the condensed phase fuel vaporizes as shown in Fig. 1 (A). When $\phi_g \leq 1$, fuel is the limiting reactant and is consumed in the reaction zone. Vaporization mainly takes place in the preheat zone, with the mass fraction of the condense phase particles (Y_s) dropping to zero and the mass fraction of the fuel vapor (Y_F) reaching a maximum in the preheat zone. The temperature increases through the preheat zone, reaches the maximum value in the reaction zone, and remains constant in the convection zone (losses are neglected).

Case II represents the conditions of $\phi_g \leq 1$ and particles do not vaporize in the preheat zone as shown in Fig. 1(B). Particles continue to burn even in the convection zone, resulting in the temperature in the convective zone (T_b) to be greater than the flame temperature (T_f). The inset labeled "*H*" in Fig. 1 shows the convection zone in case II, where the fuel particles continue to

burn in the presence of excess oxygen. The presence of these particles is mainly because of their larger sizes and/or slow vaporization rate. Note that this case results in increase of the temperature in the convection zone.

Case III represents the condition where $\phi_g \geq 1$. All the particles vaporize in the preheat zone as shown in Fig. 1 (C_I). However, in this case, only part of the gas-phase fuel burns in the flame zone, because of the fuel-richness of the mixture, and there is fuel vapor left over in the convection zone. Oxygen is the limiting reactant in this case. Assuming there are no heat losses, temperature can be approximated to remain constant in the convection zone.

Case IV represents the conditions where $\phi_g \geq 1$ and the particles are not completely vaporized in the preheat zone as shown in Fig. 1 (C_{II}). Similar to case III, oxygen is the limiting reactant for this case also. However, as the particles continues to vaporize in the convective zone, the mass fraction of the fuel vapor increases and the temperature in the convection zone decreases. The inset labeled "I" in Fig. 1 shows a close-up of the convection zone, which occurs in case IV where fuel particles continue to vaporize but do not burn because of oxygen limitation. This continued vaporization increases the fuel vapor mass fraction and decreases the convection zone temperature.

3. Mathematical model

The following main assumptions are used: (1) particle temperature and velocity same as gas, (2) burning on surface (heterogeneous) combustion is not possible, (3) constant properties, (4) ideal gas law, (5) homogeneous flame front, (6) mean molecular weight does not vary, (7) thermal conductivity of the mixture is proportional to temperature (8) diffusion coefficient is proportional to the temperature squared, (9) no radiation loss, (10) vaporization modeled using a power law, and (11) one step Arhenius gas phase reaction rate. The structure of the preheat vaporization zone is determined from a balance between the convective, diffusive, and vaporization terms in the conservation equations. As shown in Fig. 2, vaporization of fuel particles can be expected to go on in the convective zone where both gas phase chemical reaction and vaporization of fuel particles is present. The burning velocity is obtained by analyzing the reaction zone where the convective and vaporization terms are small, compared with diffusive and reactive terms. The combustion is modeled as a one-step overall reaction:

$$\nu_F[F] + \nu_O[O] \rightarrow \nu_{prod}[P] \tag{1}$$

F, O and P denote the fuel, oxidizer, and products, respectively, and ν_F,ν_O and ν_{prod} are their respective stoichiometric coefficients. The governing equations of mass, energy, and gaseous species can be written as [18]:

Mass conservation:

$$\rho u = \text{constant} \tag{2}$$

Energy conservation:

$$\rho u c_{p,mix} \frac{dT}{dx} = \lambda \frac{d^2T}{dx^2} + \dot{w}_F^{'''} \frac{\rho_u}{\rho} Q - \dot{w}_v^{'''} \frac{\rho_u}{\rho} Q_v \tag{3}$$

It is assumed that the fuel particles vaporize to form a gaseous fuel with known properties. $c_{p,mix}$ is the combined heat capacity of the gas $c_{p,g}$, and that of the particles $c_{p,s}$. A procedure to estimate its value experimentally has been discussed by Seshadri et al. [18]. The kinetics of vaporization are given by, $\dot{w}_v^{'''} = An_s 4\pi r^2 T^n$ and the gas phase reaction rate is given by $\dot{w}_F^{'''} = \nu_F W_F k C_F$. n_s = number of particles per unit volume, r = radius of fuel particle, and T = temperature. A and n are constants, which can be obtained. For example, the rate parameters characterizing the kinetics of vaporization of coal dust are calculated as $A = 3.4 \times 10^{-6}$ g/cm^2-K/s and $n = 1.33$, from the rate of volatilization of coal at $T = 1400$ K, reported by Coffee et al. [19]. Gas-phase fuel species conservation is given by:

$$\rho u \frac{dY_F}{dx} = \rho_u D_u \frac{d^2 Y_F}{dx^2} - \dot{w}_F^{'''} \frac{\rho_u}{\rho} + \dot{w}_v^{'''} \frac{\rho_u}{\rho} \tag{4}$$

where D_u is the diffusivity assumed to be equal to $\lambda_u/(\rho_u c_{p,g})$(Lewis number = 1 is assumed).

Mass fraction, Y_s of the particles is given by:

$$\rho u \frac{dY_s}{dx} = -\dot{w}_v^{'''} \frac{\rho_u}{\rho} \tag{5}$$

Boundary conditions for Eqs. (3)–(5) are:

$Y_F = 0, T = T_u$, and $Y_s = Y_{Fu}$ at $x \rightarrow -\infty$ and $Y_F = \text{finite}$, $T = T_b$, at $x \rightarrow \infty$.

T_b, is the final adiabatic temperature in the convective zone and $Y_{Fu} = 4\pi r_u^3 n_u \rho_s/(3\rho_u)$represents the mass fraction of fuel available in the particles (subscript u, denotes conditions at ambient). In the limit, Zeldovich number, $Ze = (E(T_f - T_u))/RT_f^2 \rightarrow \infty$, an expression for the laminar burning velocity is derived by Seshadri et al. [18] as:

$$S_L{}^2 = \frac{2\nu_F \lambda_u B (1/Ze)^2}{\rho_u c_{p,mix}} \exp\left(-\frac{E}{RT_f}\right) \tag{6}$$

Eq. (6) (depicted in Table 1) allows analysis of the controlling parameters that govern flame propagation in a uniform cloud of volatile particles. Besides the initial particle radius and number density or concentration, the kinetics of vaporization, thermal conductivity, specific heat and initial temperature T_u, also play an important role in flame propagation in a dust cloud (the sensitivity of each of these parameters is discussed in Section 4.4).

The set of equations discussed in (1)–(6) is valid for scenario B in Fig. 1 and can be applied to scenario A with suitable assumptions. However, the model is not suitable in the oxygen limited cases C_I and C_{II}. We extend and validate the model to represent the cases C_I and C_{II} where $\phi_g \geq 1$ as shown in Fig. 1 by setting $\nu_F = \nu_O$,$B = B/\nu_O$ and $T_f = T_b$ and substituting in the equation for S_L (a list of model equations is provided in Table 1, row 2). The "switch" between lean and rich conditions is based on the adiabatic convection zone temperature (T_b). This is equal to the value where the lean adiabatic flame temperature (T_f) equals T_b and is called T^*. Once oxygen becomes the limiting reactant the flame temperature is assumed to remain constant and therefore an upper limit for calculating T_f is also imposed. The adiabatic convection zone temperature (T_b) of a gas phase reaction is calculated using an equilibrium solver based on minimizing free energy (GASEQ) assuming the products of combustion are CO_2, H_2O, CO, and excess fuel. The condense phase equivalence ratio (ϕ_u), can be calculated using,

$$\phi_u = \frac{Y_{Fu}}{Y_{air}} \Big/ \left(\frac{Y_{Fu}}{Y_{air}}\right)_{st} \tag{7}$$

In the above equation, Y_{air}represents the mass fraction of air. The ratio $(Y_{Fu}/Y_{air})_{st}$ at stoichiometric conditions is estimated as:

$$\left(\frac{Y_{Fu}}{Y_{air}}\right)_{st} = \left(\frac{m_F/m_{total}}{m_{air}/m_{total}}\right)_{st} = \left(\frac{m_F}{m_{air}}\right)_{st} = \left(\frac{\nu_F W_F}{\nu_{air} W_{air}}\right)_{st} \tag{8}$$

Table 2
Property values for coal dust.

A	3.4×10^{-6} g/(cm^2/s/K)	n	1.33 [–]	Q	1.55×10^4 cal/g
B	3.5×10^6 1/(mol/s)	ρ_s	1 g/cm^3	W_F	16 g/mol
$c_{p,s}$	1.357 cal/(g/K)	ν_F	1[–]	W_O	32 g/mol
E	23×10^3 cal/mol	ν_O	2[–]	r_s	10×10^{-6} m
λ_s	9.5×10^{-5} cal/(cm/s/K)				

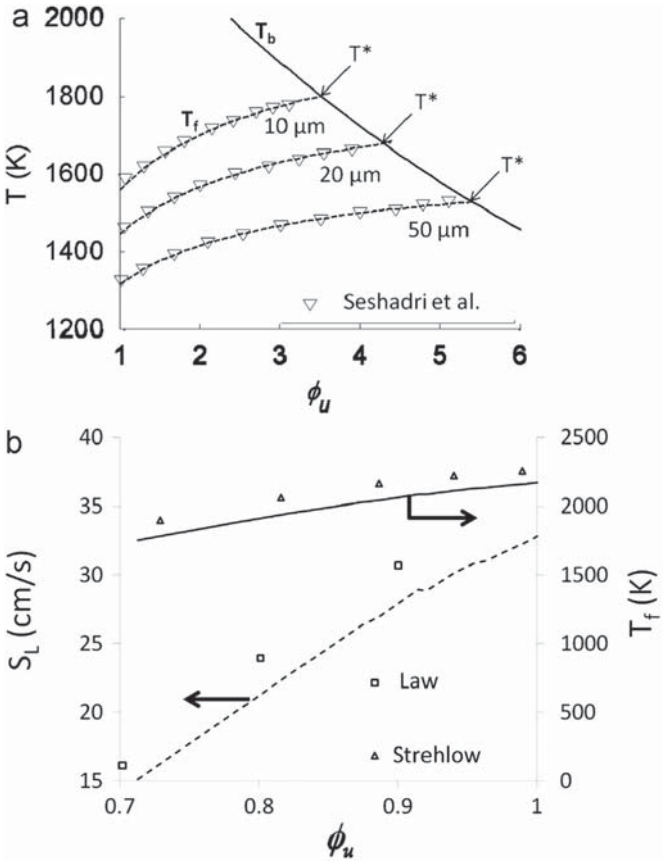

Fig. 3. Model validation (a) T_f versus φ_u calculated in this work compared with published results by Seshadri et al. [18]. (b) Comparison with experimental data for gas–air mixtures (particle size was kept extremely small (~1 μm).

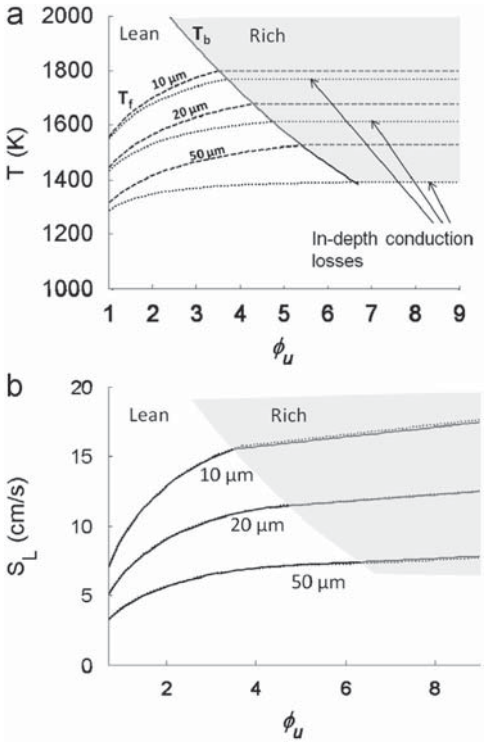

Fig. 4. Parametric study of model results (a) T_f versus φ_u for both lean and rich conditions using models 1 and 2 listed in Table 1. (b) S_L versus φ_u for both lean and rich conditions using models 1 and 2 listed in Table 1.

and

$$Y_{Fu} = 1 - Y_{air} \tag{9}$$

therefore

$$\phi_u = \frac{Y_{Fu}}{1-Y_{Fu}} \left(\frac{\nu_F W_F}{\nu_{air} W_{air}} \right)_{st}^{-1} \tag{10}$$

For simplicity in calculation, it is assumed that dust particles volatize to form methane (CH_4), which may be reasonable for coal dust. The one-step reaction is

$$CH_4 + 2(O_2 + 3.76N_2) \rightarrow CO_2 + 2H_2O + 7.52N_2 \tag{11}$$

giving $(\nu_F W_F / \nu_{air} W_{air})_{st}^{-1} = 17.18$, and by substituting into Eq. (10)

$$\phi_u = 17.18 \frac{Y_{Fu}}{1-Y_{Fu}} \tag{12}$$

Other properties such as gas-phase reaction kinetic parameters (B and E), condensed-phase vaporization kinetic parameters (A and n), thermal conductivity, specific heat, and densities are reported in Table 2 and are used to estimate the laminar burning velocity for different concentrations of the dust–air mixture. The next section discusses the results and their interpretation.

4. Results and discussion

4.1. Validation

The system of equations that represent each model (Table 1) are solved using a non-linear least squares approach. Fig. 3a shows the temperature of the reaction – zone (T_f) and convection – zone (T_b) plotted as a function of ϕ_u. The data from Seshadri et al. [18] is represented by triangular symbols showing the solution methodology used (T_b values and mathematical model) is correct. Fig. 3a shows that T_f increases as ϕ_u increases up to an optimum condition such that $T_f = T_b$. When this condition is reached (marked as T^* in Fig. 3a), the burning velocity is calculated using the equations reported in the second row of Table 1. The reason that T^* decreases with increasing particle size is because for the same concentration, as particle diameter increases, its surface area decreases, thereby reducing the fuel vaporization rate that ultimately influences the energy production rate.

Further validation of the model is achieved by estimating the behavior of a pure gas-air premixed flame (no dust). This is achieved by lessening the particle radius or by increasing the vaporization parameters (A or n) to make the particles approach a gas-air system (both options produce similar results). Fig. 3b shows the calculated laminar burning velocity (S_L) and flame temperature (T_f) compared to experimental data for a pure methane-air flame reported by Law [20] and Strehlow et al. [21]. The model shows good agreement with experiment data. It predicts the laminar burning velocity (within 10%) and flame temperature (within 5%) of a methane-air gas flame.

4.2. Oxygen limiting condition

Fig. 4a shows T_f as a function of ϕ_u for both lean and rich conditions using the equations listed in Table 1. The effect of particle size on T_f is also shown in this figure. Properties of coal dust (reported in Table 2) are used in the analysis. As the particle size is increased, from 10 μm to 50 μm, T_f reduces from a peak of 1700 K to 1500 K. The oxygen limited condition is analyzed by switching the solution method to represent the fuel-rich condition shown in Table 1, row 2 when $T_f = T^*$ is reached. Fig. 4b shows the effect of ϕ_u on the laminar burning velocity (S_L) for 10 μm, 20 μm, and 50 μm coal particles. Note that the dust–air-flame shows no decay in velocity as ϕ_u increases in the range of equivalence ratios

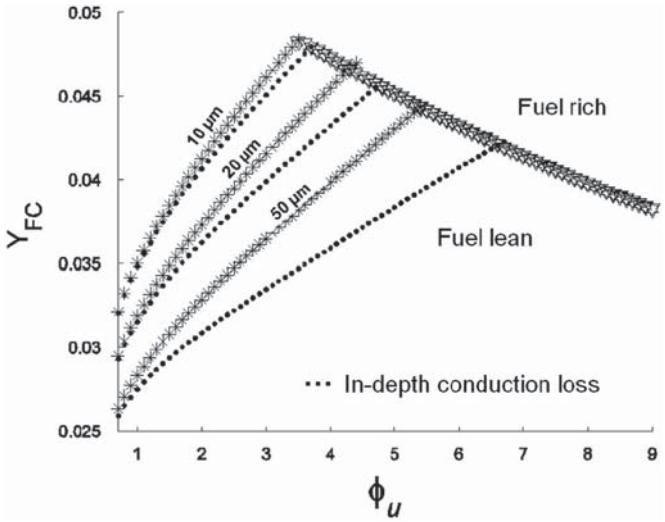

Fig. 5. Mass fraction of fuel vapor versus φ_u.

shown. In the fuel lean model, S_L increases as ϕ_u increases mainly due to the similar increase in T_f as discussed in Fig. 4a. For example, at $\phi_u=1$, the 10 μm particles have a value of S_L which is 5 cm/s higher than the 50 μm particles and the velocity of the 10 μm particles increases (as a function of ϕ_u) at a rate 4 times higher than the 50 μm particles. The increase of both the magnitude and the rate of change of S_L is due to the higher surface area to volume ratio available at the smaller particle sizes. In the oxygen limited model (depicted by the gray shaded region in Fig. 4a and b), S_L remains almost constant for the larger particle sizes (50 μm) and increases slightly for smaller particle sizes (10 and 20 μm). This behavior is further analyzed during comparison with experimental data discussed later in Fig. 6.

Also shown in Fig. 4a is the influence of thermal lag which causes the particle temperature to be slightly less than the gas temperature. The dotted lines shown in Fig. 4a and b are calculated using the model discussed by Bidabadi and Rahbari [22] who incorporate the influence of heat losses due to in-depth conduction. Note that while the thermal lag has a significant influence on the flame temperature, its effect on burning velocity is minimal. This is explained by the trend of fuel vapor mass fraction (Y_{FC}) shown in Fig. 5.

Fig. 5 shows the effect of ϕ_u on the fuel vapor mass fraction (Y_{FC}) for 10 μm, 20 μm, 50 μm coal particles. In the fuel lean condition ($T_f < T^*$) Y_{FC} increases as ϕ_u increases. This trend reverses in the oxygen limiting condition. The decrease in the fuel vapor mass fraction counteracts the increase in temperature, which is why S_L remains almost a constant in the oxygen limited region.

4.3. Comparison with experimental data

The model is compared with experiments involving dust–air flames performed in a constant volume (20 l) explosion spheres as described in ASTM E1226 [23]. Cashdollar [24] obtained an expression to obtain the burning velocity of a dust–air mixture using the explosion sphere given by:

$$S_L = \frac{K_{st}}{4.84((P_{max}/P_0)-1)P_{max}} \quad (13)$$

where P_{max} is the experimentally determined peak pressure recorded in the constant volume explosion sphere. High accuracy is not achieved using this method because of neglecting the igniter effects and turbulence created during the initial mixing. However, qualitative trends can be gained. Besides, burning velocity of a

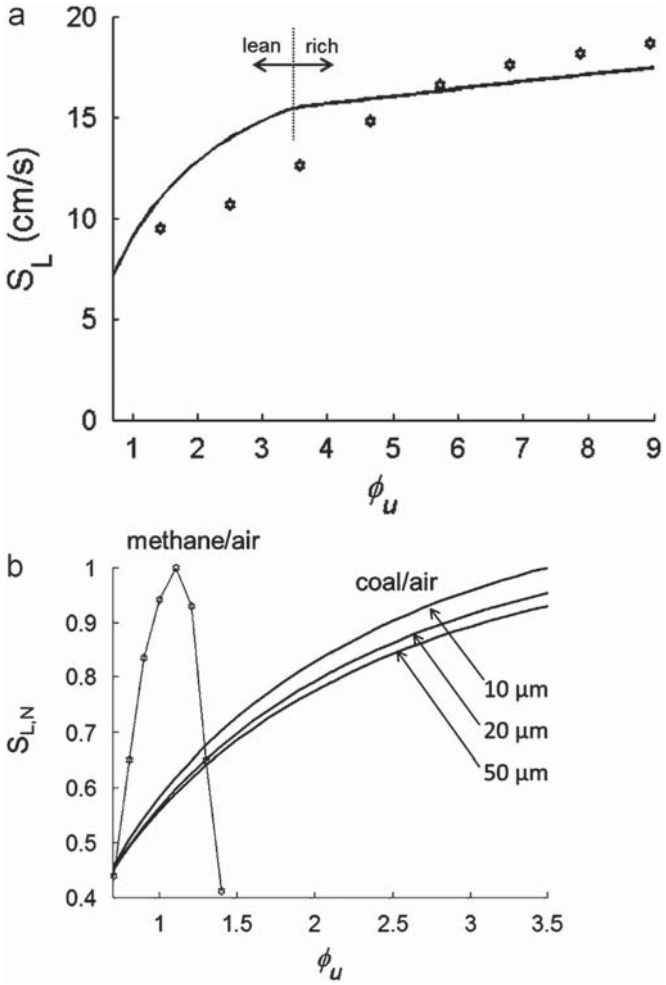

Fig. 6. Comparison of model output with experimental data. (a) S_L calculated using model 1 and 2 compared with experimental data for coal (b) Normalized laminar burning velocity S_{LN} versus φ_u for Methane gas and model 1 using coal particles ranging from 10 μm to 50 μm. $S_{LN}=S_l/S_{Lmax}$.

Table 3
Laminar burning velocity for coal–dust–air flames (coal dust concentration $=200$ g/m^3).

	S_L (cm/s)	Particle size (μm)
This work	12	10
Strehlow et al. [21]	14	40
Burgoyne and Long [26]	9	11

flammable spray, toxic gas mixture with unfavorable optical properties or a dust–air flame is difficult to obtain using more accurate methods such as counterflow burners and no experimental data currently exists [25]. Fig. 6a shows calculated burning velocities for both lean and rich conditions, respectively. Also shown is the experimental data for coal by Cashdollar [24] where Eq. (13) is used in conjunction with K_{st} values obtained in the 20-l explosion sphere.

Particle sizes used in the experiments performed by Cashdollar [24] are not reported, but based on test protocol can be assumed to be in the range of 10–100 μm with an average size of 70 μm. Both gas and condensed phase properties of coal dust were obtained from Seshadri et al. [18] and reported in Table 2. Fig. 6a shows that the model results qualitatively match experimental data. As mentioned earlier an exact match is not possible because of the inaccuracies associated with both the measurement process

Table 4
Input variables used in sensitivity analysis (Fig. 7).

ϕ	1[−]
A	3.4×10^{-6} g/(cm^2/s/K)
B	3.5×10^{6} 1/(mol/s)
$c_{p,g}$	0.24 cal/(g/K)
$c_{p,s}$	1.357 cal/(g/K)
E	23×10^{3} cal/mol
λ_u	3.5×10^{-4} cal/(cm/s/K)
λ_s	9.5×10^{-5} cal/(cm/s/K)
n	1.33 [−]
Q	0.05 [−]
ρ_u	1.77×10^{3} g/cm^3
ρ_s	1 g/cm^3
ρ_g	ρ_u g/cm^3
T_u	300 K
R	1.994 cal/(K/mol)
υ_F	1[−]
υ_O	2[−]
Q	1.55×10^{4} cal/g
W_F	16 g/mol
W_O	32 g/mol
r_s	10×10^{-6} m

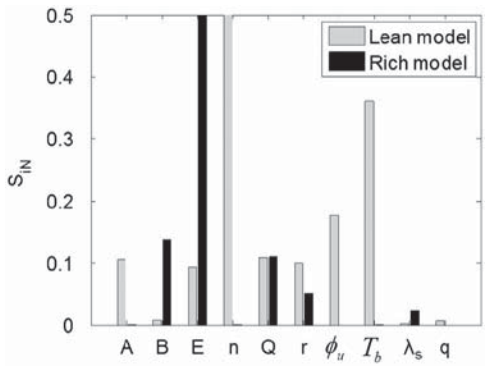

Fig. 7. Sensitivity analysis of laminar burning velocity for lean and rich conditions.

(explosion sphere) and assumptions used in the model (one step kinetics, constant property assumptions, no radiation losses etc.) However, the model clearly captures the experimental trend. The burning velocity increases initially and then levels off at higher equivalence ratios. The switch between the lean and rich condition using the adiabatic flame temperature discussed earlier is necessary to model oxygen-limited conditions. As discussed earlier, S_L does not decay as ϕ_u increases in both the experiment and model results which are in contrast to gas flames which show distinct flammability limits.

Table 3 shows comparison of the model with experimental data by Strehlow et al. [21] and Burgoyne and Long [26]. Reasonable agreement is observed. Both experiments used a Bunsen-burner type experimental set up obtaining burning velocity of a coal–dust–air flame using the cone-angle method, though only for limited concentrations.

Fig. 6b shows the laminar burning velocity of a methane-air flame compared with a coal–dust–air flame. The upper and lower flammability limits of a methane flame are shown in sharp relief compared with the ability of the dust flame to propagate through high concentrations of dust. As discussed by Eckhoff [1] and Ju et al. [27], dust explosions can occur with concentrations over two to four orders of magnitude at stoichiometric. From an industry hazard perspective this means there is a wide range of dangerous concentrations of dust which can cause an explosion.

4.4. Sensitivity analysis

Table 1 shows that the burning velocity of a premixed particle-air flame is controlled by several parameters such as vaporization rate, particle size, number density etc. To explore the controlling parameters, a sensitivity analysis is performed on the presented models using Saltelli et al. [28]. A sensitivity parameter (S_i) is defined as:

$$S_i = \frac{\ln(y_{1,i})-\ln(y_{0,i})}{\ln(x_{1,i})-\ln(x_{0,i})} \tag{14}$$

where, x_0 and x_1 are the initial and final values of the parameter to be examined, and y_0 and y_1 are the corresponding model solutions in burning velocity. The normalized sensitivity analysis value (S_{iN}) is calculated by dividing the calculated S_i value by $S_{i,max}$, representing the largest value calculated for the model. The normalized sensitivity is used to distinguish the controlling parameters of the fuel lean (scenario A or B shown in Fig. 1) and fuel rich models (C_I and C_{II} scenarios shown in Fig. 1). The model representing each and listed in Table 1 is tested using a constant set of parameters listed in Table 4. Each parameter alters by 5% and the resulting sensitivity is shown in Fig. 7.

Results show that in the scenarios representing $\phi_g<1$ as shown in (cf. Fig. 1, cases A and B) the exponent of the vaporization kinetic term (n) and convection zone temperature (T_b) are the most dominant in determining the burning velocity. Thus, for $\phi_g<1$ the vaporization-rate is controlling the rate of the overall combustion. In scenarios C_I and C_{II}, as shown in Fig. 7, the activation energy of the gas-phase reaction (E) is the most dominant followed by the frequency factor (B) and the heat of the reaction (Q). This is because of the fact that when $\phi_g>1$ the system is oxygen controlled and, therefore the terms related to the rate of the gas phase reaction are the controlling parameters. The burning velocity is not sensitive to the equivalence ratio based on the total condensed phase fuel in the ambient zone, ϕ_u in the oxygen limited case. This is observed and discussed in Fig. 4b as well. The particle size or particle radius is slightly more dominant for the fuel lean case as shown in Fig. 7. On the other hand, the thermal conductivity of the dust is more influential in the case of an oxygen controlled flame front. The influence of heat of gasification is incorporated using $S_{L,q}=S_L\exp(-qZe/2)$ where $S_{L,q}$ is the burning calculated including the heat of gasification (cf. Seshadri et al. [18] for derivation) and q is the ratio of heat of gasification to heat of reaction (assumed to be small). It is observed that q may have some influence on the burning velocity in the lean case, but is not significant in the rich case.

5. Conclusions

Modeling of premixed flammable dust–air flames is presented. A model for predicting the burning behavior of high concentration dust flames is compared with experimental data showing reasonable agreement. The need for considering two equivalence ratios in dust flames is explained along with the use of the convection zone temperature as the upper limit under certain conditions. A sensitivity analysis performed in this study shows that when $\phi_g<1$ the burning velocity is mainly dependent on the vaporization of the fuel but when $\phi_g\geq1$ the gas phase reaction kinetics play the most dominant role.

Acknowledgements

The authors would like to thank the National Science Foundation for funding this work (NSF award #0846764).

References

[1] R.K. Eckhoff, Dust Explosions in the Process Industries, Gulf Professional Publishing, Boston, 2003.
[2] T. Abbasi, S.A. Abbasi, Dust explosions–cases, causes, consequences, and control, J. Hazard. Mater. 140 (1) (2007) 7–44.
[3] OSHA, Hazard Communication Guidance for Combustible Dusts, 2009.
[4] Nusselt, W., Die Verbrennung und die Vergasung der Kohle auf dem Rost. 1924. 68: 124.
[5] D. Smoot, M.D. Horton, Propagation of laminar pulverized coal-air flames, Prog. Energy Combust. Sci. 3 (1977) 235–258.
[6] J.L. Krazinski, R.O. Buckius, H. Krier, Coal dust flames:a review and development of a model for flame propagation, Prog. Energy Combust. Sci. 5 (1979) 31–71.
[7] S.E. Slezak, R.O. Buckius, H. Krier, A modle of flame propagation in rich mixtures of coal dust in air, Combust. Flame 59 (1985) 251–265.
[8] C. Proust, Flame propagation and combustion in some dust–air mixures, J. Loss Prev. Process Ind. 19 (2006) 89–100.
[10] Y. Huang, G.A. Risha, V. Yang, R.A. Yetter, Combustion of bimodal nano/micro-sized aluminum particle dust in air, Proc. Combust. Inst. 31 (2007) 2001–2009.
[11] J. Sun, R. Dobashi, T. Hirano, Structure of flames propagating through aluminum particles cloud and combustion process of particles, J. Loss Prev. Process Ind. (2006) 769–77319 (2006) 769–773.
[12] M.D. Horton, F.P. Goodson, L.D. Smoot, Characteristics of flat, laminar coal–dust flames, Combust. Flame 28 (1977) 187–195.
[13] A. Dahoe, Dust explosions: a study of flame propagation, Applied Sciences, Delft University of Technology, 2000, p. 298.
[14] M.F. Bardon, D.E. Fletcher, Dust explosions, Science Progress (Oxford) 68 (1983) 459–473.
[15] F.A. Williams, Combustion Theory, Addison-Wesley, 1965.
[16] S. Goroshin, M. Kolbe, J.H.S. Lee, Flame speed in a binary suspension of solid fuel particles, Proc. Combust. Inst. 28 (2000) 2811–2817.
[17] L.V. Boichuk, V.G. Shevchuk, A.I. Shvets, Flame propagation in two-component aluminum–boron gas suspensions, Combust. Explos. Shock Waves 38 (6) (2002) 651–654.
[18] K. Seshadri, A.L. Berlad, V. Tangirala, The structure of premixed particle-cloud flames, Combust. Flame 89 (1992) 333–342.
[19] T.P. Coffee, A.J. Kotlar, M.S. Miller, The overall reaction concept in premixed, laminar, steady-state flames. I. stoichiometries, Combust. Flame **54** (1) (1983) 155–169.
[20] C.K. Law, Combustion Physics, Cambridge University Press, 2006.
[21] Strehlow, R.A., L.D. Savage, S.C. Sorenson, Coal dust combustion and suppression, in: AIAA/SAE 10th Propulsion Conference, San Diego, CA, 1974.
[22] M. Bidabadi, A. Rahbari, Modeling combustion of lycopodium particles by considering the temperature difference between the gas and the particles, Combustion, Explosion, and Shock Waves 45 (3) (2009) 278–285.
[23] ASTM-E1226 Standard Test Method for Pressure and Rate of Pressure Rise for Combustible Dusts, 2010, American Society for Testing and Materials (ASTM).
[24] K.L. Cashdollar, Overview of dust explosibility characteristics, J. Loss Prev. Process Ind. 13 (2000) 183–199.
[25] A. Dahoe, L.De Goey, On the determination of the laminar burning velocity from closed vessel gas explosions, J. Loss Prev. Process Ind. 16 (6) (2003) 457–478.
[26] J.H. Burgoyne, V.D. Long, Some measurements of the burning velocity of coal-in-air suspensions, in: Conference on Science in the use of coal, 1958.
[27] W. Ju, R. Dobashi, T. Hirano, Dependence of flammability limits of a combustible particle cloud on particle diameter distribution, J. Loss Prev. Process Ind. 11 (1998) 177–185.
[28] A. Saltelli, K. Chan, E.M. Scott, Sensitivity Analysis, John Wiley & Sons, LTD., 2000.